Desalination and Water Treatment
www.deswater.com

doi:10.5004/dwt.2019.23523

141 (2019) 187–196
February

Enhanced adsorption of 2, 4-dichlorophenoxyacetic acid from aqueous medium by graphene oxide/alginate composites

Asaad F. Hassan

Department of Chemistry, Faculty of Science, University of Damanhour, Damanhour, Egypt, Tel. +201005105504, email: asmz68@yahoo.com (A.F. Hassan)

Received 19 June 2018; Accepted24 November 2018

ABSTRACT

Calcium alginate beads (A), graphene oxide (GO) and GO/alginate beads composites (GA1, GA2 and GA3) as solid adsorbents were prepared and characterized by thermogravimetric curves (TGA), nitrogen adsorption/desorption curves, point of zero charge (pH_{PZC}), X-ray difffractometer (XRD), transmission electron microscope (TEM) and Fourier-transform infrared spectroscopy (FTIR). Adsorption of 2, 4-dichlorophenoxyacetic acid as one of the most toxic applied herbicide in the fields worldwide was studied considering the effect of different adsorption parameters. Results revealed that the optimum adsorbent dosage and initial pH value were found 2.0 g/L and pH 6, respectively. Freundlich and Langmuir adsorption models were applied and the maximum adsorption capacity was confirmed by GA3 (150.4 mg/g). Kinetic and thermodynamic studies proved that the adsorption follows the pseudo-second order kinetic models (PSO) and the exothermic spontaneous physisorption process.

Keywords: Graphene oxide; Alginate; Composite; Herbicide; Adsorption

1. Introduction

Graphene oxide (GO) and graphene as a carbon content nanomaterial have attracted many researchers interest in the field of catalysis, energy saving, electronic [1], mechanics and environmental applications [2,3]. Graphene oxide exhibits the graphene skeleton with oxygen function groups, such as hydroxyl and 1, 2-epoxides function groups located at the basal planes and carboxyl, hydroxyl and carbonyl groups at the edge of GO sheets [4,5].

GO has been used in removal of many organic and inorganic pollutants [6–8] with higher adsorption capacity due to its surface function groups. After water treatment by GO it is difficult to remove the spent adsorbent because it disperses well in water [9]. There are many attempts that were done to facilitate GO removal from aqueous medium after adsorption process such as, mixing with magnetic nanoparticles, functionalization and composite formation with other materials [10,11]. Alginate is a natural biopolymer mainly extracted from brown seaweed with a linear polysaccharide composing of 1, 4-linked residues of α-L-guluronic acid and β-D-mannuronic acid. Alginate has been considered as promising biomaterial due to its nontoxicity, the presence of many function groups, biodegradability and water solubility. Many applications were developed for alginate including drug delivery [12], tissue engineering [13], wound dressing [14] and solid stable adsorbents [15]. 3D macro-composites based on GO and biopolymers are superb formulations in water treatment due to their unique physical, mechanical, chemical and textural properties. 2, 4-dichlorophenoxyacetic acid is one of the most extensively applied herbicide in controlling the broad-leaved weeds in fields worldwide [16]. 2, 4-D is moderately toxic with allowable concentration of 0.1 mg/L in potable water [17]. Different methods have been studied for pesticides removal such as photo-Fenton treatment [18], aerobic degradation, photocatalytic degradation [19] electrodialysis [20], advanced oxidation processes [21] and adsorption [22]. Adsorption process has been widely used in removal of pollutants from polluted waters due to its simplicity and low cost technique [23].

*Corresponding author.

In this work, the preparation and characterization of GO/alginate composites with different GO: alginate ratios is investigated. The effect of different parameters, such as adsorbent dosage, solution pH, initial concentration, shaking time and temperature on the removal of 2, 4-D will be evaluated. On the other hand, kinetic and thermodynamic parameters will be examined to understand the nature of adsorption process. To the best of my knowledge, adsorption of 2, 4-D by GO/alginate beads composites was not studied up to now.

2. Materials and methods

2.1. Materials

Graphite powder with particle size about 30 nm, 2, 4-D and sodium alginate were purchased from Sigma-Aldrich Co., Ltd., $CaCl_2$ was purchased from Alfa-Aesar Co. Ltd. Other chemicals used in the experiments were purchased from El-Nasr for pharmaceutical and chemical industrial Co., Egypt and used without further treatment.

2.2. Preparation of solid adsorbents

Graphene oxide was prepared using Hummers method [24] with some modification. 0.5 g $NaNO_3$ and 0.5 g of graphite powders were mixed in an ice bath, 50 mL of concentrated sulfuric acid (98%) was added to the previous mixture and kept under stirring, 0.5 g of potassium permanganate was added gradually to the mixture with keeping its temperature below 20°C. The mixture's temperature was raised gradually to 35°C with continuous stirring for 3 h followed by slow addition of 60 mL double distilled water. An amount of 5.0 mL of 30% hydrogen peroxide was added to the mixture till the formation of brilliant yellow residue. The residue was washed by 10% HCl solution and deionized water to remove the residual acid. The resulted graphene oxide sample (GO) was carefully dried at 75°C under vacuum for 12 h.

Calcium alginate beads were prepared by using sodium alginate treated with calcium chloride as described in detail in previous works [15,25]. Sodium alginate solution (1%, w/v) was added drop-by-drop to $CaCl_2$ solution (3%, w/v). Calcium alginate beads (A) washed several time with deionized water to remove excess $CaCl_2$. The previous beads were dried at 75°C for 12 h.

GO/alginate composites were prepared with different graphene oxide/alginate percentage (5, 10 and 20% from graphene oxide, namely; GA1, GA2 and GA3, respectively). It was prepared by ionic gelation method where certain weight of fine powder graphene oxide was dispersed in 50 mL of deionized water and stirred with 100 mL of sodium alginate for 2 h. The previous mixture was added stepwisely from 100 mL burette into 3%, w/v aqueous solution of calcium chloride and the formed solid adsorbents was washed and dried as described in the preparation of alginate beads.

2.3. Characterization of the prepared solid adsorbents

Thermal gravimetric analysis as essential characterization technique was studied to identify the thermal behavior of GO, A, GA1, GA2 and GA3 using Shimadzu DTA-50 (Japan). Specific surface area (S_{BET}, m^2/g), average pore radius (nm) and total pore volume (V_p, cm^3/g) were determined for all the solid adsorbents using nitrogen adsorption at –196°C via NOVA2000 gas sorption analyzer (Quantachrome Corporation, USA). XRD patterns (Cu Kα, λ = 1.5418 Å) were obtained for all the prepared solid material samples using a D8 advance diffractometer (Bruker AXS, Germany). The microstructures of GO, A and GA2 were investigated using transmission electron microscope (JEOL JEM-2100F TEM). pH_{PZC}(point of zero charge) for GO, A, GA1, GA2 and GA3 was determined by: initially, 30 mL of 0.01 M sodium chloride solutions were added into several closed bottles. The pH for each bottle was adjusted to a value between 2 and 12 by 0.01 M HCl and/or 0.01 M NaOH, and then a portion of the sample (0.25 g) was added to each solution, the bottles were agitated for 72 h and the final pH was then measured. The pH_{PZC} is the point where $pH_{final} - pH_{initial}$ = zero. Chemical surface function groups were measured using Mattson 5000 FTIR spectrometer in the range between 4000 and 400 cm^{-1} for all the prepared samples.

2.4. Adsorption experiments

2.4.1. Effect of adsorbent dosage

The effect of adsorbent dosage for all the solid adsorbents was investigated in the range of 1.0–4.0 g/L at pH 7, 600 mg/L as initial adsorbate solution concentration, 6 h as shaking time and at 25°C. The removal% was calculated using Eq. (1):

$$R\% = \frac{C_i - C_e}{C_i} \times 100 \quad (1)$$

where C_e and C_i are the equilibrium and initial concentration of aqueous 2,4-D solutions, respectively.

2.4.2. Effect of initial pH of adsorbate solution

The effect of pH on the initial adsorbate solution was carried out for all the investigated samples at a pH range of 1–9 using 0.01 M HCl and/or 0.01 M NaOH to adjust the required value of pH at 2.0 g/L as adsorbent dosage, after 6 h of shaking time, 600 mg/L as initial concentration of 2, 4-D solution and at 25°C.

2.4.3. Effect of initial adsorbate concentration

The effect of initial 2, 4-D concentration was tested for GO, A, GA1, GA2 and GA3 at room temperature in the concentration range 20–500 mg/L, using 2.0 g/L as adsorbent dosage, at pH 7 and 6 h as contact time. The residual 2, 4-D concentration was measured at a wavelength of 283 nm using UV–visible spectrophotometer (UV-1700 Shimadzu, Japan). The adsorption capacity (q_e, mg/g) was calculated using Eq. (2):

$$q_e = \frac{C_i - C_e}{m} \times V \quad (2)$$

where V is the volume of 2, 4-D solution (L) and m is the mass of solid adsorbent (g). Linear Langmuir adsorption

model was used to determine the maximum adsorption capacity (q_m, mg/g). Eq. (3) represents Langmuir adsorption equation.

$$\frac{C_e}{q_e} = \frac{1}{bq_m} + \frac{C_e}{q_m} \tag{3}$$

where b (L/mg) is Langmuir constant. Dimensionless separation factor (R_L) is an important parameter to investigate adsorption isotherm using the following equation [26]:

$$R_L = \frac{1}{1 + bC_i} \tag{4}$$

The type of adsorption isotherm is favourable if $0 < R_L < 1$, unfavourable when $R_L > 1$ or irreversible in case of $R_L = 0$.

Freundlich adsorption isotherm model was also performed for adsorption of 2, 4-D by all the solid adsorbents. It can be expressed as:

$$\ln q_e = \ln K_F + \left(\frac{1}{n}\right)\ln C_e \tag{5}$$

where n and K_F (mg/g (L/mg)$^{1/n}$) are the Freundlich constants which are characteristic for the system and represents on the adsorption intensity and the adsorption capacity, respectively. It is known that when the value of $1/n$ is lower than unite, it indicates a normal Langmuir isotherm; otherwise, it is an indicative of cooperative adsorption [27].

2.4.4. Effect of shaking time

The effect of contact shaking time was carried out for GA2 and GA3 at 2.0 g/L as adsorbent dosage, pH 7, 800 mg/L as initial adsorbate concentration at 25°C. After different time intervals from 1.0 to 20 h, 1.0 mL of supernatant solution was removed to determine the residual 2, 4-D concentration as previously discussed. Time adsorption capacity (q_t, *mg/g*) was determined by Eq. (6):

$$q_t = \frac{(C_i - C_t)V}{m} \tag{6}$$

where C_t (mg/L) is the liquid-phase concentration of 2, 4-D at time t. Pseudo-first (PFO) and pseudo-second (PSO) order kinetic models [Eqs. (7), (8)] were applied to study the kinetic behavior for adsorption of 2, 4-D on GA2 and GA3.

$$\ln(q_e - q_t) = \ln(q_e) - k_1 t \tag{7}$$

$$\frac{t}{q_t} = \frac{1}{k_2 q_e^{\,2}} + \frac{1}{q_e}t \tag{8}$$

where q_e and q_t are the amounts of 2, 4-D adsorbed (mg/g) at equilibrium and at time t (h), respectively. k_1 (h^{-1}) and k_2 (g/mg. h^{-1}) are the rate constants of PFO and PSO models.

2.4.5. Effect of temperature

The effect of adsorption temperature was examined at three different temperatures 25, 30 and 40°C for adsorption of 2, 4-D by GA3. Thermodynamic parameters ($\Delta H°$, $\Delta G°$ and $\Delta S°$) were calculated using the following equations:

$$K_d = \frac{C_s}{C_e} \tag{9}$$

$$\Delta G^o = \Delta H^o - T\Delta S^o \tag{10}$$

$$\ln K_d = \frac{\Delta S^o}{R} - \frac{\Delta H^o}{RT} \tag{11}$$

where K_d is the adsorption distribution coefficient, C_s is the surface adsorbed (mg/L) and C_e is the equilibrium concentration (mg/L) of 2, 4-D in the solution. T is the absolute temperature and R is the gas constant. $\Delta S°$ and $\Delta H°$ were calculated from the intercept and slope of Van't Hoff plot [Eq. (11)].

3. Results and discussion

3.1. Characterization of the prepared solid adsorbents

Fig. 1a shows thermograms for all the solid samples up to 800°C. Calcium alginate beads exhibited a weight loss about 4% at 110°C due to the loss of surface adsorbed water molecules. The second noticeable weight loss of 24.5% was at around 270°C may be ascribed to the destruction of the alginate backbone and loss of –OH groups in the form of H_2O. Above 340°C the excessive weight loss may be attributed to alginate decarboxylation and the release of carbon dioxide gas [5,28]. Graphene oxide is thermally unstable compared with graphite due to the structure defects in GO that caused by concentrated acid oxidation [6]. For GO the weight loss at 110°C around 14.2% is higher compared with calcium alginate beads and is related to the presence of active surface functional groups. The observed weight loss over 235°C is attributed to labile oxygen-containing functional groups [5,29]. GO/alginate composites exhibited a lower thermal stability compared with that of alginate beads due to the crosslinking of GO within the matrix of alginate which was also reported in previous works [30,31]. In case of GO/alginate composites the higher thermal instability at lower temperature (110–230°C) is believed to be related to the higher thermal conductivity and destruction of oxygen containing groups and it is also confirmed by increasing in weight loss with the increase in GO percentage [32].

Nitrogen adsorption isotherms and linear BET plots for GO, A, GA1, GA2 and GA3 are shown in Figs. 1b and c, respectively. The specific surface area (S_{BET}, m^2/g), total pore volume (V_P, cm^3/g) and pore radius (nm) are listed in Table 1.Nitrogen adsorption isotherms for GO, GA1, GA2 and GA3 appear as a mixture between type I and type II according to IUPAC classification disclosing microporous–macroporous nature, while A is a pure type I. Surface area of GO is three times that of alginate beads which may be related to the very thin nature of GO sheets. Incorporation of GO into alginate matrix was accompanied with surface area increase and total pore volume in the order GA3 > GA2 > GA1 indicating that as the percentage of GO increased the porosity nature increased which may be related to the promotion of crosslinking action between alginate beads via hydrogen bonding and the formation of 3D network leading to the creation of new pores [33,34].

The XRD patterns of GO, A, GA1, GA2 and GA3 are presented in Fig. 1d. GO pattern reveals its characteristic

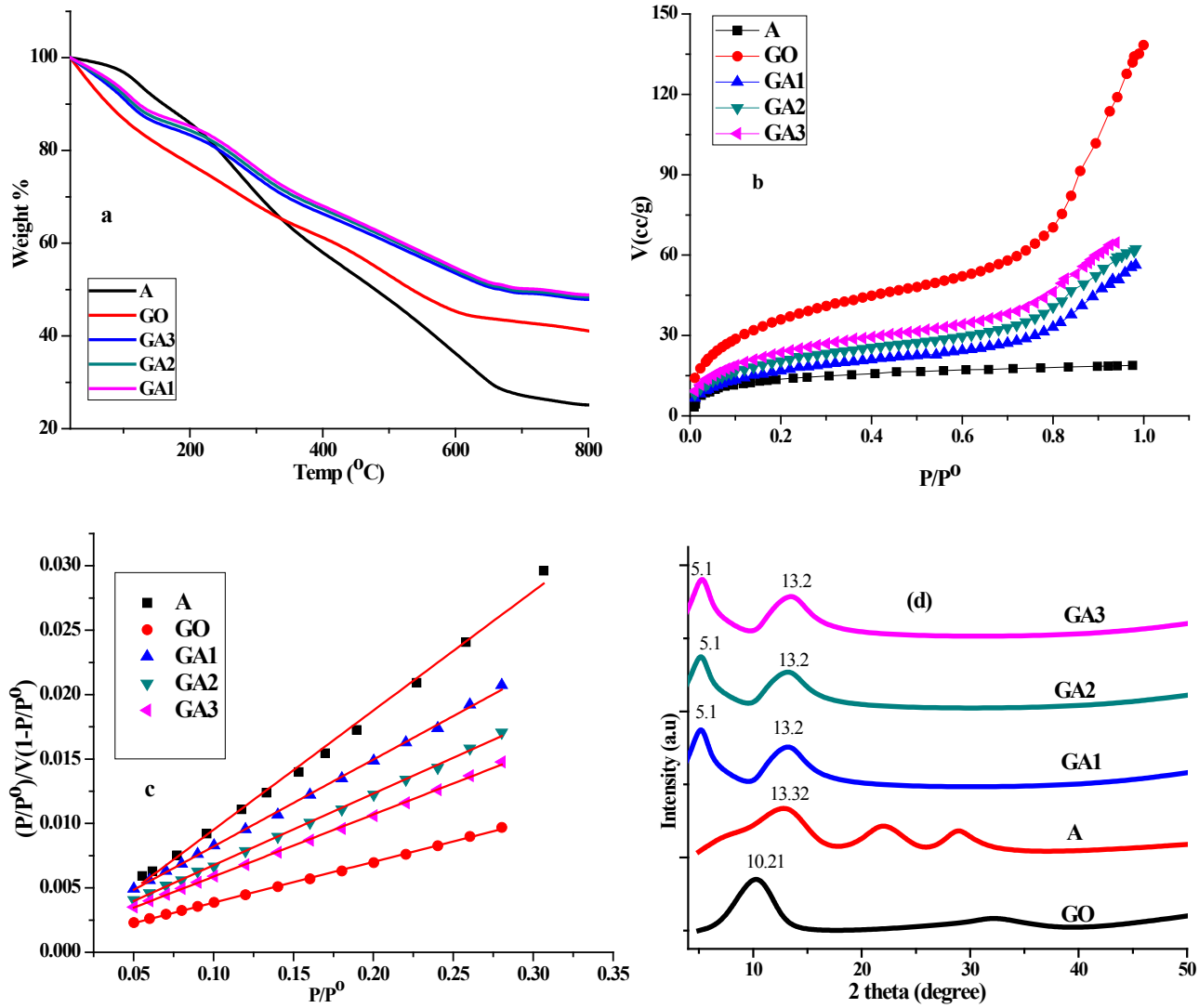

Fig. 1. TGA curves (a), nitrogen adsorption/desorption isotherms (b), BET-plot (c) and XRD of A, GO, GA1, GA2, and GA3.

Table 1
Nitrogen adsorption parameters and pH_{PZC} for all the prepared solid adsorbents

Parameters	A	GO	GA1	GA2	GA3
R^2	0.99520	0.99941	0.99891	0.99910	0.99941
S_{BET} (m^2/g)	45.2	135.1	63.5	77.7	89.9
$\bar{r}$ (nm)	1.34	3.10	2.79	2.54	2.53
V_p (cm^3/g)	0.0301	0.2093	0.0878	0.0977	0.1123
pH_{PZC}	6.1	3.5	5.8	5.5	4.9

peak at 2θ =10.21° with interplanar spacing of 0.872 nm [35]. Alginate beads shows a characteristic peaks at 2θ = 13.32° with 0.663 nm as average intermolecular distance and indicating the amorphous nature of the sample [36]. XRD results for composites (GA1, GA2 and GA3) showed two diffraction peaks at 2θ = 5.10 and 13.20° associated with GO and alginate beads. The diffraction angle of graphene oxide is shifted from 10.21 to 5.10° with an increase in d spacing from 0.872 to 1.620 nm in case of composites indicating the formation of intercalated structures [37].

Figs. 2a, b, c show TEM for GO, A and GA2, respectively. GO present as very thin smooth and homogenous sheets while alginate beads shows a spherical shape. GA2 appeared as a lamellar structure with bulky surface groups compared with GO sheets and that confirms the homogeneous distribution between alginate and GO [38].

pH_{PZC} is essential characterization parameter to discuss the adsorption behaviors of solid adsorbents. pH_{PZC} of GO, A, GA1, GA2 and GA3 are 3.5, 6.1, 5.8, 5.5 and 4.9, respectively (Table 1). The acidity of GO surface indicates the presence of different acidic C–O functional groups [39]. The surface acidity for alginate beads was found to be around the neutral point as reported in my previous work [15]. In case of GO/alginate composites, it was found that as the percentage of GO increases, the surface acidity also increased. The prepared composites (GA1, GA2 and GA3)

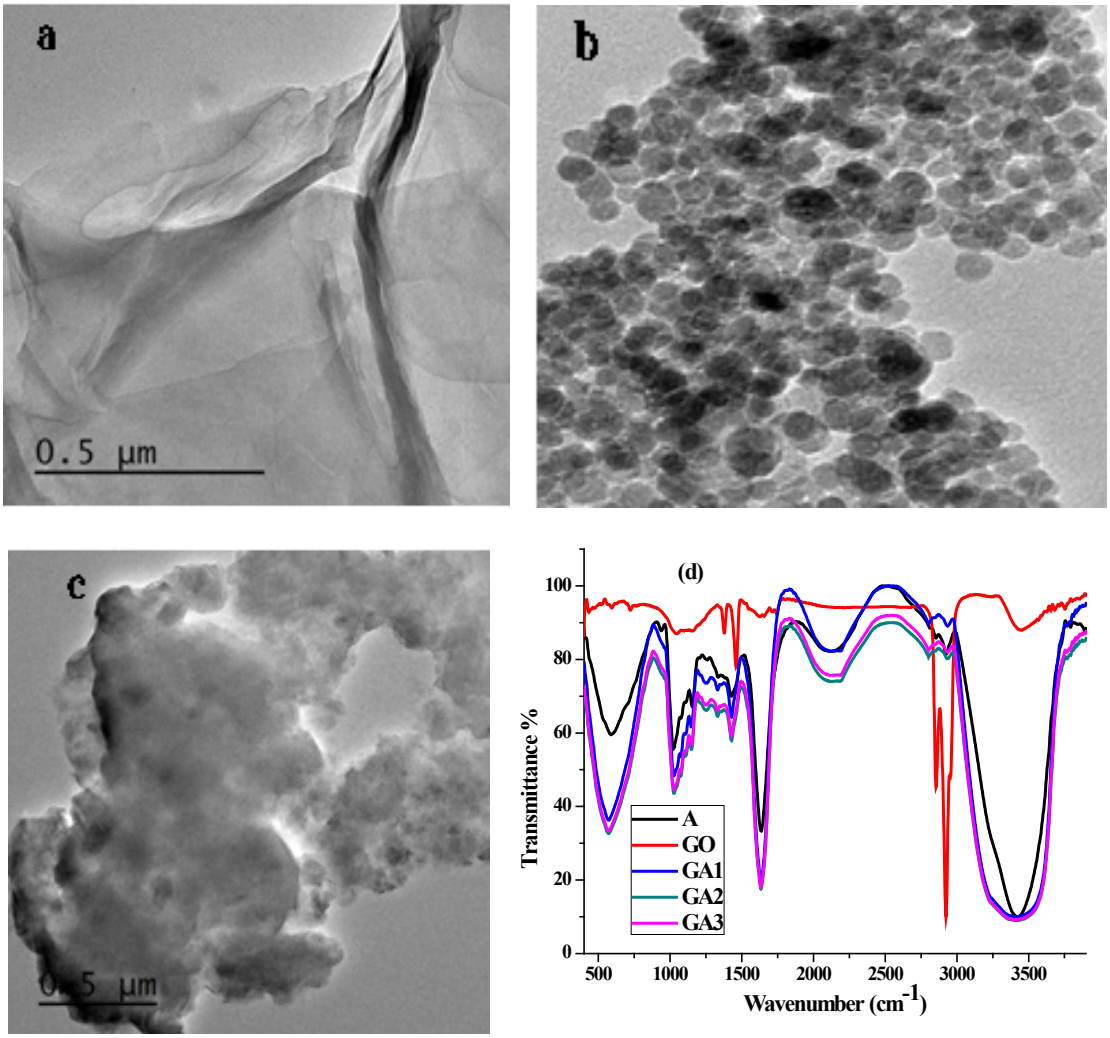

Fig. 2. TEM for GO (a), A (b), GA2 (c) and FTIR for A, GO, GA1, GA2, GA3 (d).

showed a decrease in pH_{PZC} approximately with the same percentage of mixed GO (5, 10 and 20%).

FTIR is still one of the most important techniques to understand the nature of the chemical surface groups of solid adsorbents. Fig. 2d shows the FTIR spectra for all the investigated solid samples. GO spectrum agreed with the spectrum reported in previous works [40–42].

Broad band located around 3445 cm^{-1} is related to associated and free O–H groups stretching vibrations from C–OH, COOH and H_2O. The band located at 1747 cm^{-1} might be related to C=O (carbonyl) stretching vibrations of carboxylic groups created at the edges of the oxidized graphene oxide. The bands located at 1374, 1459, 1628, 2860 and 2931 cm^{-1} corresponding to the O–H deformation vibration of carboxylic groups [43], semi-circle stretch of aromatic rings [44], stretching vibrations of C=C, C– H symmetric stretching vibration and C–H asymmetric stretching vibration of methylene groups, respectively [45]. Calcium alginate beads show their characteristic peaks at 1029, 1447, 1630, 2939, 3419 cm^{-1} which are attributed to C–O–C stretching vibration, $–CH_2$ bending, $–COO^-$ asymmetric stretching, $–CH_2$ stretching and –OH stretching, respectively [46–49]. GO/alginate composite patterns show band broadening around 3445 cm^{-1} indicating that GO interact with alginate beads through intermolecular hydrogen bonds and confirms the good miscibility between GO and alginate [33,50].

3.2. Adsorption of 2, 4-D

3.2.1. Effect of adsorbent dosage

Fig. 3 are presents the relation between adsorbent dosage and the removal percentage of 2, 4-D onto all the investigated adsorbent samples. Based on the general trend, at the beginning as the adsorbent dosage increases from 1.0 to 2.0 g/L there are observable increase in removal% for all the investigated samples (67, 95, 50, 55, and 68% for A, GO, GA1, GA2 and GA3, respectively). The reported results can be related to the increase in the number of surface adsorption active sites [51]. At higher solid adsorbent dosage (>2.0 g/L) the increase in removal% is not observed due to the establishment of adsorption equilibrium at an extremely lower 2, 4-D concentration [52]. 2.0 g/L was selected as the optimal adsorbent dosage value for all the investigated solid adsorbents.

3.2.2. Effect of pH

The initial pH value of the adsorbate solution is important factor in adsorption process. Fig. 3b predicts the removal % of 2, 4-D in the pH range 1–9. A and GA1 exhibited a constant removal % at pH < 6 and slightly decreased after that value. GO exhibited the same trend but with observable decrease in removal % at pH > 6 which may be related to the increased repulsion between the negative charge on the adsorbate molecule and the negatively charged functional groups on the solid adsorbents surface (pH > pK_a, 2.73 for 2, 4-D). In case of GA2 and GA3a sharp decrease in removal % at pH > 6 were observed due to its lower pH_{PZC} (5.5 and 4.9, respectively). In a general at pH > pK_a values, the molecules exist in the anionic forms and as the pH increases, the degree of dissociation of 2, 4-D increases and they become more negatively. At pH < pH_{pzc}, the solid surface acquires a positive charge, while at pH > pH_{pzc}, the surface has a net negative charge [17,53].

3.2.3. Effect of initial concentration of 2, 4-D

Adsorption isotherm curve represents the distribution of adsorbate molecules between solid surface and aqueous medium. Fig. 4a shows the effect of initial 2, 4-D concentration on adsorption process. The adsorption isotherms follow Type I and Type II according to BDDT (Brunauer, Deming, Deming and Teller) classification [54]. At lower concentration there are rapid increases in the adsorbed amount of 2, 4-D due to the higher ratio of surface active site/adsorbate molecules while; plateau horizontal line was observed at higher equilibrium concentration based on the saturation of solid adsorbent surface with adsorbate molecules.

Langmuir [Eq. (3)] and Freundlich [Eq. (5)] isotherm models were used to test the adsorption data. Figs. 4b, c show Langmuir and Freundlich adsorption equations while, Table 2 collects the parameters of the two models. Upon analysis of Table 2 (i), both of Langmuir and Freundlich models are applicable because of the higher regression coefficients (R^2, ranged between 0.98426–0.99954 and 0.89380–0.99646 in case of Langmuir and Freundlich, respectively). (ii) Maximum adsorption capacities (q_m, mg/g) calculated from Langmuir adsorption models indicate that GA3 shows the maximum adsorption value of 65 and 42% more than A and GO, respectively indicating that the combination between GO and alginate matrix positively affect sits adsorption capacity and

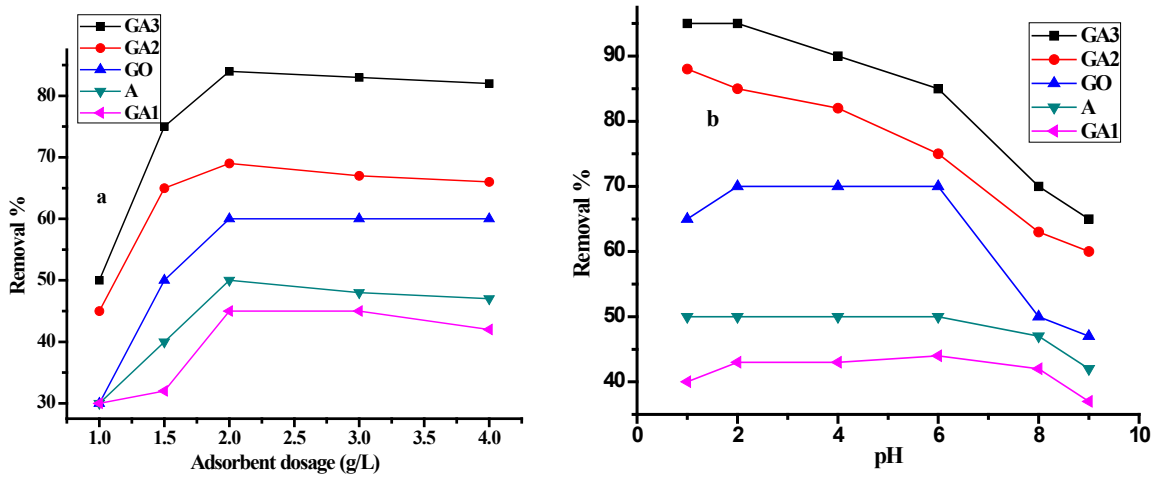

Fig. 3. Effect of initial adsorbent dosage at pH 7 (a) and the effect of pH at adsorbent dosage 2.0 g/L (b) for the adsorption of 2,4-D onto A, GO, GA1, GA2 and GA3. Adsorption conditions: initial concentration = 600 mg/L, temp. = 25°C, shaking time = 6 h.

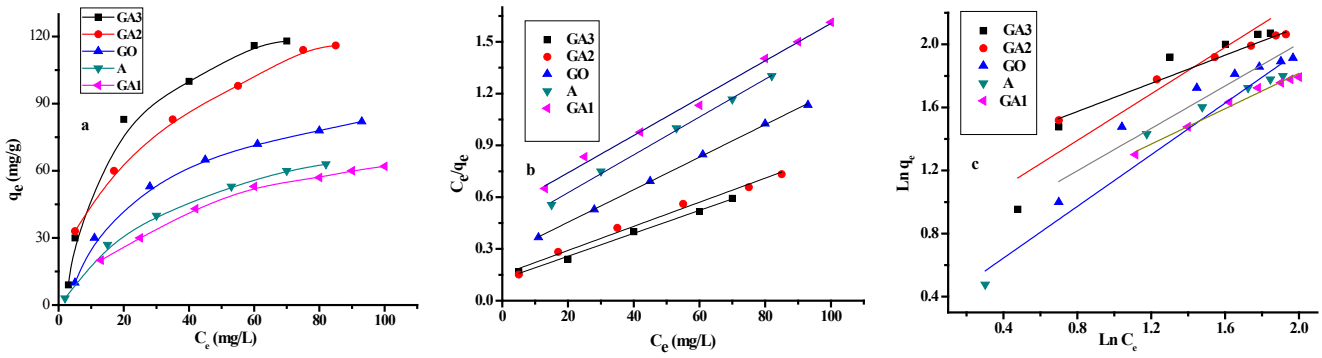

Fig. 4. Adsorption isotherms (a), linear Langmuir plot (b) and Freundlich plot (c) for the adsorption of 2, 4-D onto A, GO, GA1, GA2 and GA3. Adsorption conditions: pH 7, shaking time = 6 h, temp. = 25°C and adsorbent dosage = 2.0 g/L.

the increase in GO % in the composite is accompanied by the adsorption efficiency enhancement which may be explained by the introduction of excessive C–O function groups as adsorption active sites. (iii) R_L values for 2, 4-D adsorption onto all the solid samples were less than 1.0 and more than zero, indicating favorable adsorption process. (iv) *1/n* values ranged between 0.103 and 0.819 for the investigated solid adsorbents indicating that adsorption of 2, 4-D is in favorable conditions [55]. 2, 4-D removal via adsorption has been studied using different solid adsorbents such as commercial powdered activated carbon (PAC), modified granular activated carbon F400 (coal based), sodium hydroxide activated carbon based date palm pits (AN13), Mn oxide-humic complex, modified Jute, Orange Peel (OP) and MIEX resin [56–62]. In this study graphene oxide/alginate composite (GA3) was compared with other adsorbents (Table 3) which indicates the higher efficiency of graphene oxide/alginate composite as solid adsorbents for 2, 4-dichlorophenoxyacetic acid.

Table 2
Langmuir and Freundlich adsorption parameters for adsorption of 2, 4-D onto all theinvestigated solid adsorbents

Langmuir parameters					
Parameters	A	GO	GA1	GA2	GA3
R^2	0.99757	0.99954	0.99438	0.98426	0.99493
q_m (mg/g)	91.2	106.0	94.4	143.1	150.4
b (L/mg)	0.02699	0.03545	0.02062	0.04618	0.05345
R_L	0.2703	0.2200	0.3266	0.1779	0.1576
Freundlich parameters					
Parameters					
R^2	0.89380	0.99646	0.91234	0.95508	0.98260
$1/n$	0.735	0.447	0.672	0.819	0.103
K_F	6.319	16.471	4.578	2.077	4.949

3.2.4. Adsorption kinetics

The effect of contact time and adsorption kinetic models was studied on the adsorption of 2, 4-D by GA2 and GA3 to understand the mechanism of adsorption. Figs. 5a, b and c show the effect of shaking time, PFO and PSO kinetic models for the adsorption process, respectively. Adsorption kinetic parameter reported in Table 4 reveals that: the adsorption of 2, 4-D follow pseudo–second order kinetic models due to its higher regression coefficients (R^2, around 0.9780) also the calculated q_e (mg/g) values from PSO models are closure to the experimental values (q_{exp}) while, a large differences between the calculated q_e (mg/g) values from PFO model and q_{exp} were detected.

Table 3
Comparison of Langmuir adsorption capacities of 2,4-D onto graphene oxide/alginate composite (GA3) with other adsorbents reported in previous researches

Adsorbents	Adsorption equilibrium time (h)	q_m (mg/ g)	References
Commercial powdered activated carbon (PAC)	4.0	90.4	[56]
Modified granular activated carbon F400 (Coal based)	2.8	16.3	[57]
Sodium hydroxide activated carbon based date palm pits (AN13)	5.5	80.0	[58]
Mn oxide-humic complex	15.0	5.6	[59]
Modified Jute	2.5	38.5	[60]
Orange Peel (OP)	2.6	34.5	[61]
MIEX resin	1.1	46.9	[62]
Graphene oxide/alginate composite (GA3)	9.0	150.4	[This study]

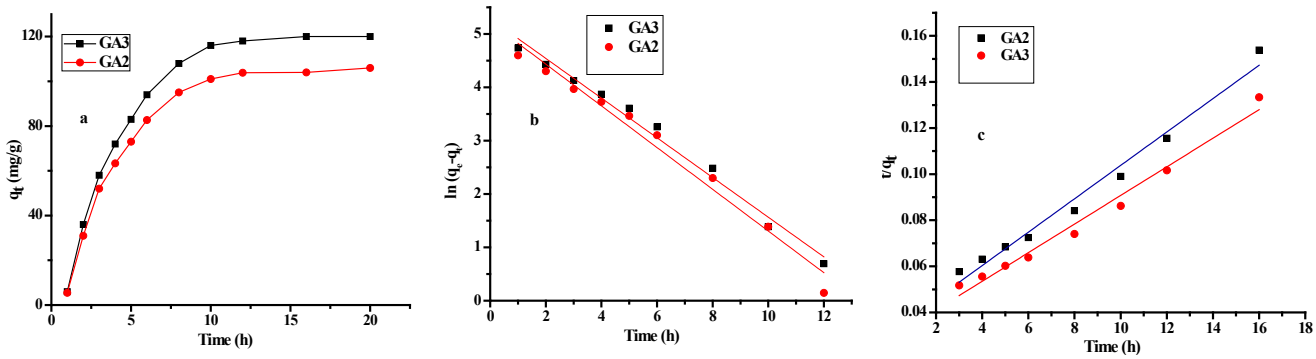

Fig. 5. Effect of contact time (a), pseudo-first order (b), and pseudo-second order plots (c) for removal of 2, 4-D by GA2 and GA3. Adsorption conditions: initial concentration = 800 mg/L, pH 7, temp. = 25°C and adsorbent dosage = 2.0 g/L.

Table 4
Pseudo-first order and pseudo-second order kinetic model parameters for adsorption of 2, 4-D onto GA2 and GA3 at 25°C

Adsorbents	q_{exp} (mg/g)	Pseudo-first order			Pseudo-second order		
		R^2	q_e (mg/g)	K_1 (h^{-1})	R^2	q_e (mg/g)	K_2 (g/mg·h^{-1})
GA2	145.0	0.94561	192	0.391	0.97864	141	0.00167
GA3	155.1	0.96471	211	0.372	0.97891	159	0.00131

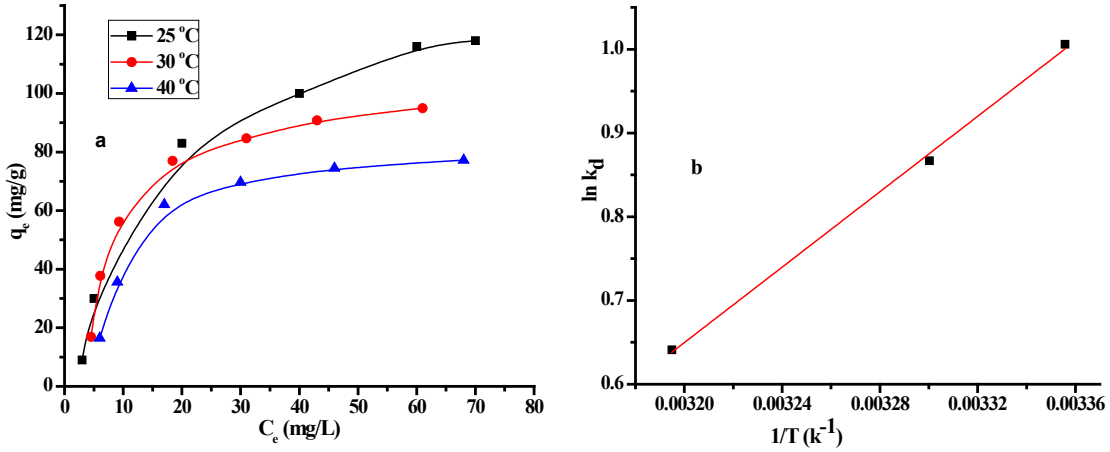

Fig. 6. Effect of adsorption temperature (a) and Van't Hoff plot for the adsorption of 2, 4-D onto GA3 at 25, 30 and 40°C. Adsorption conditions: pH 7, shaking time = 6 h and adsorbent dosage = 2.0 g/L.

3.2.5. Effect of adsorption temperature and thermodynamic parameters

The adsorption of 2, 4-D onto GA3 was examined at 25, 30 and 40°C to determine the effect of temperature and different thermodynamic adsorption parameters. Fig. 6a indicates that the adsorption capacity decreases with the increase in temperature. The calculated maximum adsorption capacities (q_m, mg/g) using Langmuir adsorption model were 150.4, 112.5 and 94.3 mg/g at 25, 30 and 40°C respectively, indicating the exothermic nature of adsorption. The calculated adsorption distribution coefficient (K_d) also confirms the decrease in affinity of 2, 4-D to GA3 surface as temperature increase where, k_d were found to be 2.729, 2.375, 1.897 at 25, 30, 40°C, respectively. Table 5 collects the thermodynamic parameters calculated using Van't Hoff equation. The higher regression coefficients (R^2, 0.99656) revealed the good applicability of Van't Hoff equation. The negative value of ΔH° confirms the exothermic nature of 2, 4-D adsorption onto GA3 sample. The positive value of entropy change demonstrates the increased randomness at the solid/liquid interface [23]. The negative values of ΔG° indicate spontaneous adsorption process. Physisorption process occurs when the magnitude of ΔG° in the range –20 and 0 kJ mol^{-1}, while chemisorption occurs between –80 and –400 kJ·mol^{-1} [5]. The calculated free energy changes for 2, 4-D adsorption onto GA3 confirms the physisorption nature.

Table 5
Thermodynamic parameters for the adsorption of 2, 4-D onto GA3 at different temperatures

ΔH° (kJ/mol)	ΔS° (kJ/mol·K^{-1})	ΔG° (kJ/mol)		
		25°C	30°C	40°C
–18.72	0.0544	–2.500	–2.237	–1.693

4. Conclusion

Graphene oxide/alginate beads were prepared with different GO: alginate ratios (GA1, GA2 and GA3). The characterization techniques proved that GO and alginate matrix were homogeneously distributed. The surface area and physical properties were improved by the introduction of GO into the matrix of alginate. GO/alginate composites showed advanced adsorption behavior towards 2, 4-dichlorophenoxyacetic acid as one of the most toxic applied herbicide in the fields worldwide. The adsorption process was fit well both of Langmuir and Freundlich adsorption models with 150.4 mg/g as adsorption capacity for GA3 sample. The adsorption follows PSO kinetic adsorption models. Thermodynamic parameters indicate that the adsorption process is exothermic spontaneous and physisorption in nature. The above mentioned results showed that GO/alginate composites are promising solid adsorbents for different types of organic herbicide.

References

[1] D. Eom, D. Prezzi, K.T. Rim, H. Zhou, M. Lefenfeld, S. Xiao, C. Nuckolls, M.S. Hybertsen, T.F. Heinz, G.W. Flynn, Structure and electronic properties of graphene nanoislands on Co(0001), Nano Lett., 9 (2009) 2844–2848.

[2] C. Lee, X. Wei, J.W. Kysar, J. Hone, Measurement of the elastic properties and intrinsic strength of monolayer graphene, Science, 321 (2008) 385–388.
[3] Y. Li, Q. Du, T. Liu, J. Sun, Y. Wang, S. Wu, Z. Wang, Y. Xia, L. Xia, Methylene blue adsorption on graphene oxide/calcium alginate composites, Carbohyd. Polym., 95 (2013) 501–507.
[4] J. Guerrero-Contreras, F. Caballero-Briones, Graphene oxide powders with different oxidation degree, prepared by synthesis variations of the Hummers method, Mater. Chem. Phys, 153(1) (2015) 209–220.
[5] P. Emiliano, E.F. Maria, R.B. Pablo, L.C. Ana, Graphene oxide/alginate beads as adsorbents: Influence of the load and the drying method on their physicochemical-mechanical properties and adsorptive performance, J. Colloid Interface Sci., 491 (2017) 1–12.
[6] T. Liu, Y. Lia, Q. Du, J. Sun, Y. Jiao, G. Yang, Z. Wang, Y. Xia, W. Zhang, K. Wang, H. Zhu, D. Wu, Adsorption of methylene blue from aqueous solution by graphene, Colloids Surf., B, 90 (2012) 197–203.
[7] S.P. Ho, O.K. Sung, Sorption behavior of slightly reduced, three-dimensionally macroporous graphene oxides for physical loading of oils and organic solvents, Carbon Lett., 18(1) (2016) 24–29.
[8] H. Zheng-Hong, Z. Xiaoyu, L. Wei, W. Ming, Y. Quan-Hong, K. Feiyu, Adsorption of Lead(II) ions from aqueous solution on low-temperature exfoliated graphene nanosheets, Langmuir, 27(12) (2011) 7558–7562.
[9] X. Li, X. Tang, Y. Fang, Using graphene oxide as a superior adsorbent for the highly efficient immobilization of Cu(II) from aqueous solution, J. Mol. Liq., 199 (2014) 237–243.
[10] S. Chowdhury, R. Balasubramanian, Recent advances in the use of graphene family nano adsorbents for removal of toxic pollutants from wastewater, Adv. Colloid. Interf., 204 (2014) 35–56.
[11] A.L. Cukierman, E. Platero, M.E. Fernandez, P.R. Bonelli, Potentialities of graphene-based nanomaterials for wastewater treatment, in: A.K. Mishra (Ed.), Smart Materials for Waste Water Applications, Wiley-Scrivener Publishing LLC, MA, United States (2016) pp. 47–86.
[12] B. Strasdat, H. Bunjes, Development of a new approach to investigating the drug transfer from colloidal carrier systems applying lipid nanosuspension-containing alginate microbeads as acceptor, Int. J. Pharm., 489 (2015) 203–212.
[13] M.X. Liu, L.B. Dai, H.Z. Shi, S. Xiong, C.R. Zhou, In vitro evaluation of alginate/halloysite nanotube composite scaffolds for tissue engineering, Mater. Sci. Eng., C, 49 (2015) 700–712.
[14] H.E. Thu, M.H. Zulfakar, S.F. Ng, Alginate based bilayer hydrocolloid films as potential slow-release modern wound dressing, Int. J. Pharm., 434 (2012) 375–383.
[15] A.F. Hassan, A.M. Abdel-Mohsen, M.G. Fouda, Comparative study of calcium alginate, activated carbon, and their composite beads on methylene blue adsorption, Carbohydr. Polym., 102 (2014) 192–198.
[16] A. Derylo-Marczewska, M. Blachnio, A.W. Marczewski, A. Swiatkowski, B. Tarasiuk, Adsorption of selected herbicides from aqueous solutions on activated carbon, J. Therm. Anal. Calorim., 101 (2010) 785–794.
[17] Z. Aksu, E. Kabasakal, Batch adsorption of 2, 4-dichlorophenoxyacetic acid (2, 4- D) from aqueous solution by granular activated carbon, Sep. Purif. Technol., 35 (2004) 223–240.
[18] A. Zapata, T. Velegraki, J.A. Sánchez-Pérez, D. Mantzavinos, M.I. Maldonado, S. Malato, Solar photo-Fenton treatment of pesticides in water: Effect of iron concentration on degradation and assessment of ecotoxicity and biodegradability, Appl. Catal. B: Environ., 88(3–4) (2009) 448–454.
[19] A.F. Hassan, H. Elhadidy, A.M. Abdel-Mohsen, Adsorption and photocatalytic detoxification of diazinon using iron and nanotitania modified activated carbons, J. Taiwan Inst. Chem. Eng., 75 (2017) 299–306.
[20] L.J. Banasiak, B.V. Bruggen, A.I. Schafer, Sorption of pesticide endosulfan by electrodialysis membranes, Chem. Eng. J., 166 (2011) 233–239.
[21] I.B. Mohamed, Y.G. Montaser, G. Tarek, Advanced oxidation processes for the removal of organophosphorus pesticides from wastewater, Desalination, 194 (2006) 166–175.
[22] A.M. Youssef, H. EL-Didamony, S.F. EL- Sharabasy, M. Sobhy, A.F. Hassan, B. Roman, Adsorption of 2, 4 dichlorophenoxyacetic acid on different types of activated carbons based date palm pits: kinetic and thermodynamic studies, Int. Res. J. Pure Appl. Chem., 14(1) (2017) 1–15.
[23] J.M. Salman, B.H. Hameed, Adsorption of 2,4-dichlorophenoxyacetic acid and carbofuran pesticides onto granular activated carbon, Desalination, 256 (2010) 129–35.
[24] W.S. Hummers, R.E. Offeman, Preparation of graphitic oxide, J. Am. Chem. Soc., 80 (1958) 1339–1339.
[25] A. Bée, D. Talbot, S. Abramson, V. Dupuis, Magnetic alginate beads for Pb(II) ions removal from wastewater, J. Colloid Interf. Sci., 362 (2011) 486–492.
[26] A.F. Hassan, H. Radim, Chitosan/nanohydroxyapatite composite based scallop shells as an efficient adsorbent for mercuric ions: Static and dynamic adsorption studies, Int. J. Biol. Macromol., 109 (2017) 507–516.
[27] L. Fan, C. Luo, M. Sun, X. Li, H. Qiu, Highly selective adsorption of lead ions by water-dispersible magnetic chitosan/graphene oxide composites, Colloids Surf., B, 103 (2012) 523–529.
[28] B. Kusuktham, P. Prasertgul, Srinun, Morphology and property of calcium silicate encapsulated with alginate beads, Silicon, 6 (2014) 191–197.
[29] J. Chen, Y. Li, L. Huang, C. Li, G. Shi, High-yield preparation of graphene oxide from small graphite flakes via an improved Hummers method with a simple purification process, Carbon, 81 (2015) 826–834.
[30] M. Yadav, K.Y. Rhee, S.J. Park, Synthesis and characterization of graphene oxide/carboxymethylcellulose/alginate composite blend films, Carbohydr. Polym., 110 (2014) 18–25.
[31] C. Jiao, J. Xiong, J. Tao, Xu, D. Zhang, H. Lin, Y. Chen, Sodium alginate/graphene oxide aerogel with enhanced strength–toughness and its heavy metal adsorption study, Int. J. Biol. Macromol., 83 (2016) 133–141.
[32] H. Zhang, X. Pang, Y. Qi, pH-Sensitive graphene oxide/sodium alginate/polyacrylamide nanocomposite semi-IPN hydrogel with improved mechanical strength, RSC Adv., 5 (2015) 89083–89091.
[33] Z. Yuan, Y. Fei, C. Junhong, M. Jie, Batch and column adsorption of methylene blue by graphene/alginate nanocomposite: Comparison of single-network and double-network hydrogels, J. Environ. Chem. Eng., 4 (2016) 147–156.
[34] T. Ma, P.R. Chang, P. Zheng, F. Zhao, X. Ma, Fabrication of ultra-light graphene based gels and their adsorption of methylene blue, Chem. Eng. J., 240 (2014) 595–600.
[35] T. Molly, S.N. Thillai, U.D.S. Mehraj, B. Mustri, K. Farid, Self-organized graphene oxide and TiO_2 nanoparticles incorporated alginate/carboxymethyl cellulose nanocomposites with efficient photocatalytic activity under direct sunlight, J. Photochem. Photobiol. A: Chem., 346 (2017) 113–125.
[36] S.G. Kim, G.T. Lim, J. Jegal, K.J. Lee, Pervaporation separation of MTBE (methyl tert-butyl ether) and methanol mixtures through polyion complex composite membranes consisting of sodium alginate/chitosan, J. Membr. Sci., 174(1) (2000) 1–15.
[37] I. Mariana, A.P. Madalina, I. Horia, Sodium alginate/graphene oxide composite films with enhanced thermal and mechanical properties, Carbohydr. Polym., 94 (2013) 339–344.
[38] F. Lihong, G. Hongyu, Z. Shengqiong, X. Yao, W. Huigao, L. Ya, F. Han, N. Min, Sodium alginate conjugated graphene oxide as a new carrier for drug delivery syste, Int. J. Biol. Macromol., 93 (2016) 582–590.
[39] L. Tian, X. Zhang, W. Qi, D. Liu, Q. Jin, J. Lin, Y. Ye, Z. Li, W. Wu, The adsorption of water-soluble ionic liquids on graphene oxide of different oxygen content. RSC Adv, 102 (2014) 58127–58901.
[40] R. Himanshu, M.N. Shalate, O.O. Adeniyi, D.S. Ntaote, W.D. Charity, B.N. Eliazer, D.D. Ezekiel, K.P. Rajiv, P. Rajiv, Synthesis of graphene oxide and its application for the adsorption of Pb^{+2} from aqueous solution, J. Ind. Eng. Chem., 47 (2017) 169–178.

[41] C.M. Willemse, Tlhomelang, K.N. Jahed, P.G. Baker, E.I. Iwuoha, Metallo-Graphene nanocomposite electrocatalytic platform for the determination of toxic metal ions, Sensors, 11 (2011) 3970–3987.
[42] X. Geng, Y. Guo, D. Li, W. Li, C. Zhu, X. Wei, M. Chen, S. Gao, S. Qiu, Y. Gong, L. Wu, M. Long, M. Sun, G. Pan, L. Liu, Interlayer catalytic exfoliation realizing scalable production of large-size pristine few-layer graphene, Sci. Rep., 3 (2013) 1134–1142.
[43] G. Shao, Y. Lu, F. Wu, C. Yang, F. Zeng, Q. Wu, Graphene oxide: the mechanisms of oxidation and exfoliation, J. Mater. Sci., 47 (2012) 4400–4409.
[44] W. Konicki, M. Aleksandrzak, D. Moszyński, E. Mijowska, Adsorption of anionic azo-dyes from aqueous solutions onto graphene oxide: Equilibrium, kinetic and thermodynamic studies, J. Colloid Interf. Sci., 496 (2017) 188–200.
[45] L. Chen, Y. Li, Q. Du, Z. Wang, Y. Xia, E. Yedinak, J. Lou, L. Ci, High performance agar/graphene oxide composite aerogel formethylene blue removal, Carbohydr. Polym., 155 (2017) 345–353.
[46] L. Sun, B. Fugetsu, Graphene oxide captured for green use: Influence on the structures of calcium alginate and macroporous alginic beads and their application to aqueous removal of acridine orange, Chem. Eng. J., 240 (2014) 565–573.
[47] N. Jiang, Y. Xu, Y. Dai, W. Luo, L. Dai, Polyaniline nanofibers assembled on alginate microsphere for Cu^{2+} and Pb^{2+} uptake, J. Hazard. Mater., 17 (2012) 215–216.
[48] W.M. Algothmi, N.M. Bandaru, Y. Yu, J.G. Shapter, A.V. Ellis, Alginate–graphene oxide hybrid gel beads: an efficient copper adsorbent material, J. Colloid. Interf. Sci., 397 (2013) 32–38.
[49] H. Daemi, M. Barikani, Synthesis and characterization of calcium alginate nanoparticles, sodium homopolymannuronate salt and its calcium nanoparticles, 19(6) (2012) 2023–2028.
[50] Y. He, N. Zhang, Q. Gong, H. Qiu, W. Wang, Y. Liu, J. Gao, Alginate/graphene oxide fibers with enhanced mechanical strength prepared by wet spinning, Carbohyd. Polym., 88 (2012) 1100–1108.
[51] M.E. Argun, S. Dursun, C. Ozdemir, M. Karatas, Heavy metal adsorption by modified oak sawdust: thermodynamics and kinetics, J. Hazard. Mater., 141 (2007) 77– 85.
[52] A.F. Hassan, H. Elhadidy, Production of activated carbons from waste carpets and its application in methylene blue adsorption: Kinetic and thermodynamic studies, J. Environ. Chem. Eng., 5 (2017) 955–963.
[53] J.M. Salman, V.O. Njoku, B.H. Hammed, Batch and fixed-bed adsorption of 2,4-dichlorophenoxyacetic acid onto oil palm frond activated carbon, Chem. Eng. J., 174 (2011) 33–40.
[54] IUPAC. Reporting physisorption data for gas/solid systems with special reference to the determination of surface area and porosity: IUPAC recommendations, Pure Appl. Chem. 57 (1985) 603–619.
[55] A.F. Hassan, A.M. Abdel-Mohsen, H. Elhadidy, Adsorption of arsenic by activated carbon, calcium alginate and their composite beads, Int. J. Biol. Macromol., 68 (2014) 125–130.
[56] A.E. Kurtoğlu, G. Atun, Competitive adsorption of 2,4-dichlorophenoxyacetic acid herbicide and humic acid onto activated carbon for agricultural water management, Desal. Water Treat., 57(53) (2016) 25653–25666.
[57] L. Temdrara, A. Addoun, A. Khelifi, Development of olive stones-activated carbons by physical, chemical and physicochemical methods for phenol removal: A comparative study, Desal. Water Treat., 53(2) (2013) 452–461.
[58] A.M. Youssef, H. EL-Didamony, S.F. EL- Sharabasy, M. Sobhy, A.F. Hassan, R. Buláneke, Adsorption of 2, 4 dichlorophenoxyacetic acid on different types of activated carbons based date palm pits: kinetic and thermodynamic studies, Int. Res. J. Pure Appl. Chem., 14(1) (2017) 1–15.
[59] C. Liu, P.M. Huang, Kinetics of 2, 4 dichlorophenoxyacetic acid (2, 4-D) adsorption by metal oxides, metal oxide –humic complexes, and humic acid, Soil Sci., 169(7) (2004) 497–504.
[60] S. Manna, P. Saha, D. Roy, R. Sen, B. Adhikari, Removal of 2,4-dichlorophenoxyacetic acid from aqueous medium using modified jute, J. Taiwan Inst. Chem. Eng., 67 (2016) 292–299.
[61] V. Okumuş, K.S. Çelik, S. Özdemir, A. Dündar, E. Kılınç, Biosorption of chlorophenoxy acid herbicides from aqueous solution by using low-cost agricultural wastes, Desal. Water Treat., 56(7) (2015) 1898–1907.
[62] L. Ding, X. Lu, H. Deng, X. Zhang, Adsorptive removal of 2,4-dichlorophenoxyacetic acid (2,4-D) from aqueous solutions using MIEX resin, Ind. Eng. Chem. Res., 51 (2012) 11226–11235.